

INTEGRAL/IBIS CENSUS OF THE SKY BEYOND 100 KEV

A. Bazzano¹, J.B. Stephen², M. Fiocchi¹, A.J. Bird³, L. Bassani², A.J. Dean³, A.M. Alizia², P. Ubertini¹,
F. Lebrun⁴, R. Walter⁵ and C. Winkler⁶

Draft version September 11, 2018

ABSTRACT

We report on the first census of INTEGRAL/IBIS detections (& 4 significance) above 100 keV based on the Core Program and public Open Time observations up to April 2005. There are 49 sources detected in the 100–150 keV band of which 14 are also seen in the 150–300 keV range. The low energy sample is dominated by X-ray binary systems of both low and high mass, but also includes 10 active galaxies. Of the binary systems that are detected above 150 keV, more than 50% are associated with black hole candidates, often reported as microquasars. The present survey results are then used to construct LogN–LogS curves for galactic and extragalactic objects in the 100–150 keV band: above a 1 mCrab sensitivity limit we expect that around 200 galactic sources and almost 350 active galaxies populate the sky above 100 keV. While the contribution of individual point sources to the total Galactic emission has been estimated to be around 70–80% between 100–300 keV, we find that active galaxies detected above 1 mCrab account for only about 3% of the cosmic hard X-ray background in the 100–150 keV band.

Subject headings: surveys | galaxies: active | gamma rays: observations

1. INTRODUCTION

One of the primary goals of the INTEGRAL observatory (39), and in particular of the IBIS imager (38), is to provide a survey of the high energy sky (> 20 keV). To this end a number of teams have made an effort to provide a systematic analysis of the data sets, as available to them at the time, so as to provide the general community with consolidated source information: so far 2 general surveys (6; 7), several surveys of specific areas of the sky (30; 32; 28; 23) and a few AGN catalogues (4; 1) have been published. A common factor throughout all of these activities is that the source search concentrated on the 18–100 keV regime where the IBIS sensitivity to point sources is optimal. Emission at higher energies has not been specifically investigated for or characterised in terms of source typology and emission mechanism except for a few objects. In this letter we focus our search above 100 keV and report the first census of the sky above this energy; as a result we provide for the first time the LogN–LogS relationship for galactic and extragalactic sources in the 100–150 keV band as well as an estimate of the galactic source contribution to the total Galactic emission and of the AGNs to the cosmic hard X-ray background.

2. PRE-INTEGRAL SOFT X-RAY SKY

The first ever attempt to survey the sky at high energy (26–1200 keV) was performed with the Sky Survey Instrument on ArielV (14), which provided the first, and

to date only, galactic LogN–LogS relation above 100 keV. This was followed by the HEAO 1-A4 survey in the 40–180 keV band (24). Of the 44 sources detected, 14 had a formal statistical significance > 4 in the 80–180 keV band, i.e. well above the sensitivity limit of 36 mCrab. The 14 objects detected comprise 6 low mass X-ray binaries (LMXB), 4 high mass X-ray binaries (HMXB), 3 active galactic nuclei (AGN) and the Crab. Two of the LMXB sources were at that time associated with A1742–294, near the Galactic Centre, and GX 5–1. Subsequent observations by SIGMA/GRANAT detected 2 persistent black hole candidates (BHC) close to these sources that were probably responsible for the detected high energy tails. Assuming that these new identifications are correct, we can categorize the HEAO-A4 binary compact objects as 6 BHCs, 2 neutron stars (NS) and 2 objects without a clear identification so far. A further step in our knowledge of the high energy sky was provided by the SIGMA sky survey (31) which contains 37 sources of which only 6 were detected in the 100–200 keV band (5 black holes and the Crab).

A further insight into the high energy regime was provided by a catalogue of 309 sources assembled from the literature (25). Most (189) of these were gamma ray emitters, detected only above 1 MeV. Of the remainder, only 50 were reported to emit above 100 keV and these include several X-ray Novae (e.g. Nova Muscae, GRO 0422+32) sporadically detected only when arising once or twice per decade. The high sky coverage of the GRO-BATSE experiment provided a list of around 50 objects in the 70–160 keV band (21). The list is dominated by X-ray binaries both of low and high mass; however a few AGN are also reported together with supernova remnant/pulsar associations. At higher energies ($E > 700$ keV), the GRO/COMPTEL survey (33) lists 32 persistent sources including various types of galactic objects and 9 AGN. The galactic sources are divided into spin-down pulsars (7), Cygnus X–1, the Nova GRO J0422+32, 3 unidentified EGRET objects and the Crab. The extragalactic sources

¹ IASFRoma/INAF, via Fosso del Cavaliere 100, I-00133 Roma, Italy; angela.bazzano@iasf-roma.inaf.it

² IASFBologna/INAF, Via Gobetti 101, I-40126 Bologna, Italy;

³ School of Physics and Astronomy, University of Southampton, Southampton S017 1BJ, UK;

⁴ CEA-Saclay, DAPNIA/Service d'Astrophysique, F-91191 Gif-sur-Yvette Cedex, France;

⁵ Geneva Observatory, INTEGRALSDC, Chemin de l'Ecologie 16, 1291 Versoix, Switzerland;

⁶ ESA-ESTEC, RSSD, Keplerlaan 1, 2201 ZANoordwijk, Netherlands;

are all Balzars except for Cen A. This survey also reported sky regions where MeV emission features are observed. These detections, when compared to those in the hard X-ray domain, clearly indicate that there is a transition region where accreting mechanics are not longer dominant (except in the brightest sources) while synchrotron processes become important and nucleosynthesis starts taking place. This transition region is still largely unexplored despite its potential importance; this paper is an attempt to start filling in this observational gap.

3. SPI/INTEGRAL

Analysis of the first year of SPI data (8) resulted in a list of 63 hard X-ray point sources detected in the 25-50 keV band during the Galactic Plane Survey and Galactic Center Deep Exposure; only 20 sources were detected in the 50-150 keV band (above 4 σ) and 4 sources (above 5 σ) in the 150-300 keV band. One main objective of this study was to provide a direct estimate of the source contribution to the diffuse galactic emission, which was estimated to be around 90% at 100 keV while above 250 keV, diffuse electron-positronium emission dominates over the discrete source component. This result is in substantial agreement with IBIS/ISGRI data which indicate that in the 20 to 200 keV range the known binary sources account for 86% to 74% of the total galactic emission (23).

4. IBIS DATASET AND ANALYSIS

The data used herein belong to the Core Program and public Open Time observations and span from revolution 46 (February 2003) to revolution 309 (April 2005) inclusive; this represents a significant extension both in exposure time and sky coverage with respect to the second IBIS catalogue (7) with more than 4000 extra pointings (8 Ms) being analysed. A detailed description of the data analysis and source extraction criteria can be found in the above reference, the only difference being the use of an updated version (4.2) of the standard OSA software. For this search we have used the 100-150 and 150-300 keV flux maps and have adopted a 4 σ significance threshold level for the source extraction; this is lower than the 5 σ level used in the general source search but is justified by the a posteriori confirmation that all detected sources have a low energy counterpart. Sources detected only occasionally, e.g. in one or two revolutions only, are not considered in the present sample. Staring data (which are noisier than dithering observations), early exposures performed with the instrument set-up not finalized and poor quality data (including solar flares, telemetry gaps, etc.), were not included in the present mosaic. For each excess, the flux extracted from the 100-150 and 150-300 keV light curves was then used to estimate the source strength with the use of a normalization factor extracted from the Crab calibration data-set. The light curves were used for the flux extraction as they provide a more reliable result than the mosaic, and also provide a confirmation of the source detection. Once a list of reliable excesses was produced, we proceeded to identify the sources responsible for the emission. We find that all excesses have a counterpart at lower energies and all objects reported in this survey were already detected below 100 keV.

5. THE HIGH ENERGY IBIS SKY

In Table 1 we list the 49 sources seen in the 100-150 keV band of which 14 are also detected in the 150-300 keV range. The table provides the key parameters such as the source name, type and average fluxes for the 20-40, 40-100, 100-150 and 150-300 keV band in mCrab. In the two (highest) bands of interest, 1 mCrab corresponds to 3.2 and 4.8 10^{-12} erg cm $^{-2}$ s $^{-1}$ respectively. The 2 lower bands are given so as to have a consistent set of data updated with respect to that reported in Bird et al. (7). Also, BeppoSAX detections above 100 keV are reported in order to provide a flux comparison. The 49 sources listed have also been checked against studies reporting specific and more detailed analyses and the associated references are also provided. We find substantial agreement between our fluxes and those previously reported taking into account expected source variability. In our high energy catalogue we have 35 accreting galactic objects (26 LMXBs, 6 HMXBs, 2 Anomalous X-Ray Pulsar (AXPs) and 1 Soft X-Ray Repeater (SGR)), 3 isolated pulsars, 10 AGNs and 1 unidentified source suggested to be a possible BHC in a LMXB (13). It is interesting to note that while in the 100-150 keV band various source types are detected, the higher band is totally dominated by BHCs. In Fig. 1, we plot the hardness ratios, HR2 versus HR1, where HR1 is defined as the ratio of the 40-100 keV to the 20-40 keV flux and HR2 as the ratio of the 100-150 keV to the 40-100 keV flux. It is evident from the figure that there is a range of hardness ratios. The two hardest sources (upper right corner) are anomalous X-ray pulsars while the softest object is Sco X-1.

6. THE SOURCE DISTRIBUTION AND LOGN-LOGS

Even though the number of sources in this sample is limited, it is still useful to construct the logN-logS number flux relationship particularly as the sky above 100 keV is still virtually unexplored. With so few sources, it serves more as a tool with which to estimate the total number of objects which will become visible as the survey becomes more complete than as an instrument with which to study the spatial distribution. Apart from the paucity of sources, there are other complications involved in forming this relationship. The sensitivity limit in any direction depends on the exposure at that point, and is extremely non-uniform due to the pointing strategy of INTEGRAL (7). Furthermore, for the case of galactic sources, there is a strong relationship between the intrinsic distribution of the sources and the exposure, while the source list consists of an ensemble of several distinct populations (LMXBs, HMXBs etc.) each of which have different logN-logS parameters (16).

Given these caveats, we first convert exposure to 1 limiting sensitivity using the relationship shown in Fig. 2, between the flux errors and effective exposure for the sources used in this study. From this we obtain the sky coverage as a function of 4 limiting flux as shown in Fig. 3. We then create the Yaw' logN-logS for both the 10 AGNs and the 39 Galactic sources independently. These distributions are corrected for the exposure limit and sky coverage using two methods. The first is model independent (or, rather, assuming an isotropic underlying distribution), while the second assumes a model distribution based on the observed sources. Fig. 4 shows the results for the AGN. Both the Yaw' data and the corrected values normalized to full sky coverage are shown

where the horizontal bars indicate the errors on the flux of the N^{th} source. Unsurprisingly, for the AGN we find that the best model and the isotropic cases are identical (i.e. the best model is an isotropic distribution). The best-fit power law relationship and the (1 σ) statistical limits are indicated by the solid lines and are given by $N(>S) = (340 \pm 12)S^{-1.34 \pm 0.04}$. The slope is slightly flatter than the expected value of 1.5, but we can cross-check the number by making reference to the HEAO-1A4 results for the 80–180 keV all-sky survey. The limiting flux of this survey was 36 mCrab, and from our relationship we would expect to see 3 ± 1 AGN above that flux over the whole sky, in agreement with the 3 listed in the A4 catalogue (3C 273, NGC 4151 and Cen A). In Fig. 5 the results for the 39 galactic sources are shown. The best-fit relationship is given by $N(>S) = (206 \pm 3)S^{-0.84 \pm 0.01}$. The quoted errors are purely statistical, but some idea of the systematic error can be obtained by comparing this fit with that assuming a-priori an isotropic source distribution. This leads to $N(>S) = (206 \pm 23)S^{-0.84 \pm 0.06}$. Once again this can be tested by comparing the predictions for a full-sky survey at the sensitivity of the HEAO-A4 instrument. At 36 mCrab we should expect to see 10 ± 2 galactic sources while there are 11 in the A4 catalogue. The slope is very similar to that obtained for the LMXB sources in the 20–100 keV band from the first IBIS catalogue (16), which is to be expected as 26 of the 39 galactic sources in this sample are LMXBs.

7. CONCLUSIONS

A further use of the present catalogue is to estimate the contribution of galactic point sources to the total Galactic emission and that of AGN to the cosmic diffuse background in the energy bands explored in the present paper. The total galactic point source contribution has been estimated by summing the 100–150 keV fluxes from

all sources detected within the central radius excluding all AGNs and Sco-X1 which is located at high galactic latitude. The flux obtained amounts to $2.17 \pm 0.01 \times 10^{-4}$ and $4.29 \pm 0.10 \times 10^{-5}$ ph cm⁻² s⁻¹ keV for 100–150 and 150–300 keV respectively; this implies a contribution of 83% and 68% in the two bands in agreement with previous and current INTEGRAL results (8; 23). The percentage contribution does not increase much as we go to fainter fluxes as sources a factor of 100 weaker will bring the point source component to 85% contribution. The above estimates further confirm previous indications that point sources largely dominate the total Galactic emission. In a similar way, the extragalactic logN–logS distribution derived from the present survey provides a total AGN emissivity above 1 mCrab of $0.003 \text{ keV cm}^{-2} \text{ keV}^{-1} \text{ s}^{-1} \text{ sr}^{-1}$ in the 100–150 keV or approximately 3% of the total intensity of the extragalactic hard X-ray background in the same energy band (19). Extrapolation of our LogN–LogS by a factor of 100 towards fainter fluxes will account for 15% of the extragalactic background above 100 keV; this value increases to 20% if we adopt a LogN–LogS slope of 1.5. In short we just start to uncover the source populations responsible for the hard X-ray background. As the INTEGRAL mission lifetime is extended (so far confirmed till 2010), more sky will be surveyed and more exposure will be accumulated resulting in an increase in the number of objects detected. At a limiting flux of 1 mCrab (which is likely reachable in the entire lifetime of the mission) around 200 galactic objects may be detected and more than 300 AGN identified at high energy.

This research was supported by the Italian Space Agency under contract I/023/05

REFERENCES

- Bassani, L. et al. 2006, *ApJ*, 636, L65
 Beckmann, V., Gehrels, N., Favre, P., Walter, R., Courvoisier, T., J-L., Petrucci, O., Malzac, J., 2004, *ApJ*, 641, 647
 Beckmann, V., Shrader, C. R., Gehrels, N., Soldi, Lubinski, P., Zdziarski, A., Petrucci, O., Malzac, J., 2005, *ApJ*, 634, 939
 Beckmann, V., Gehrels, N., Shrader, C. R. & Soldi, S. 2006, *ApJ*, 638, 642
 Belloni, T. et al. 2006, *MNRAS*, 367, 1113
 Bird, A. J. et al. 2004, *ApJ*, 607, L33
 Bird, A. J. et al. 2006, *ApJ*, 636, 765
 Bouchet, L., Roques, J.P., Mandrou, P., Strong, A., Diehl, R., Lebrun, F. & Terrier, R. 2005, *ApJ*, 635, 1103
 Cadolle BelM., et al. 2004, *A & A*, 426, 659
 Cadolle BelM., et al. 2006, *A & A*, 446, 591
 Camero Azzar, A., Wilson, C. A., Connel, P., Martinez Nunez, S., Bay, P., Beckmann, V., Reigero, V., 2005, *A & A*, 441, 261
 Capitanio F. et al. 2005, *ApJ*, 622, 503
 Capitanio F. et al. 2006, *ApJ*, 643, 376
 Coe, M. J., Carpenter, G. F., Engel, A. R. & Quenby, J.J. 1982, *MNRAS*, 200, 385
 Courvoisier, T. J-L. et al. 2003, *A & A*, 411, L343
 Dean, A. J. et al. 2005, *A & A*, 443, 485
 DelSanto, M. et al. 2005, *A & A*, 433, 613
 DeRosa, A. 2005, *A & A*, 438, 121
 Guber, D. E., Matsson, J.L., Peterson, L. E. & Jung, G. V. 1999, *ApJ*, 520, 124
 Hannikainen D. C. et al. 2005, *A & A*, 435, 995
 Hamon B. A. et al. 2004, *ApJS*, 154, 585
 Kuiper L., Hermsen, W., den Hartog, P., Collmar, W., 2006, *ApJ* in press
 Lebrun, F. et al. 2004, *Nature*, 428, 293
 Levine A. M. et al. 1984, *ApJS*, 54, 581
 Maccomb D. J. and Gehrels N. 1999, *ApJS*, 120, 335
 Mareghetti S., Gotz, D., Mirabel, F., Hurley, K., 2005, *A & A*, 433, L9
 Molkov S. et al. 2003, *A & A*, 411, L357
 Molkov, S.V., Cherepashchuk, A. M., Lutovinov, A. A., Revnivtsev, M. G., Postnov, K. A. & Sunyaev, R. A. 2004, *Astronomy Letters*, 30, 534
 Pottschmidt, K., Chemyakova, M., Zdziarski, A., Lubinski, P., Smith, D. H., Bezzay, N., *A & A*, 452, 285
 Orr A. et al. 2004, *ESA SP-552*, 357
 Revnivtsev, M. G. et al. 2004a, *Astronomy Letters*, 30, 382
 Revnivtsev, M. G. et al. 2004b, *Astronomy Letters*, 30, 527
 Revnivtsev, M. G., Sazonov, S.Yu., Molkov, S.V., Lutovinov, A. A., Churazov, E. M. & Sunyaev, R. A. 2006, *Astronomy Letters*, 32, 145
 Shaw, S., Chemyakova, M., Rodriguez, J., Walter, R., Kretschmar, P., Mareghetti, S., 2004, *A & A*, 426, L33
 Schonfelder, V. et al. 2000, *A & A*, 143, 145
 Stumer S. J. and C. R. Shrader 2005, *ApJ*, 625, 923
 Tarana, A. et al. 2006, *A & A*, 448, 336
 Tomack, J. A. et al. 2005, *ApJ*, 630, 413
 Vilhu O. et al. 2003, *A & A*, 411, L405
 Ubertini P. et al. 2003, *A & A*, 411, L131
 Winkler C. et al. 2003, *A & A*, 411, L1

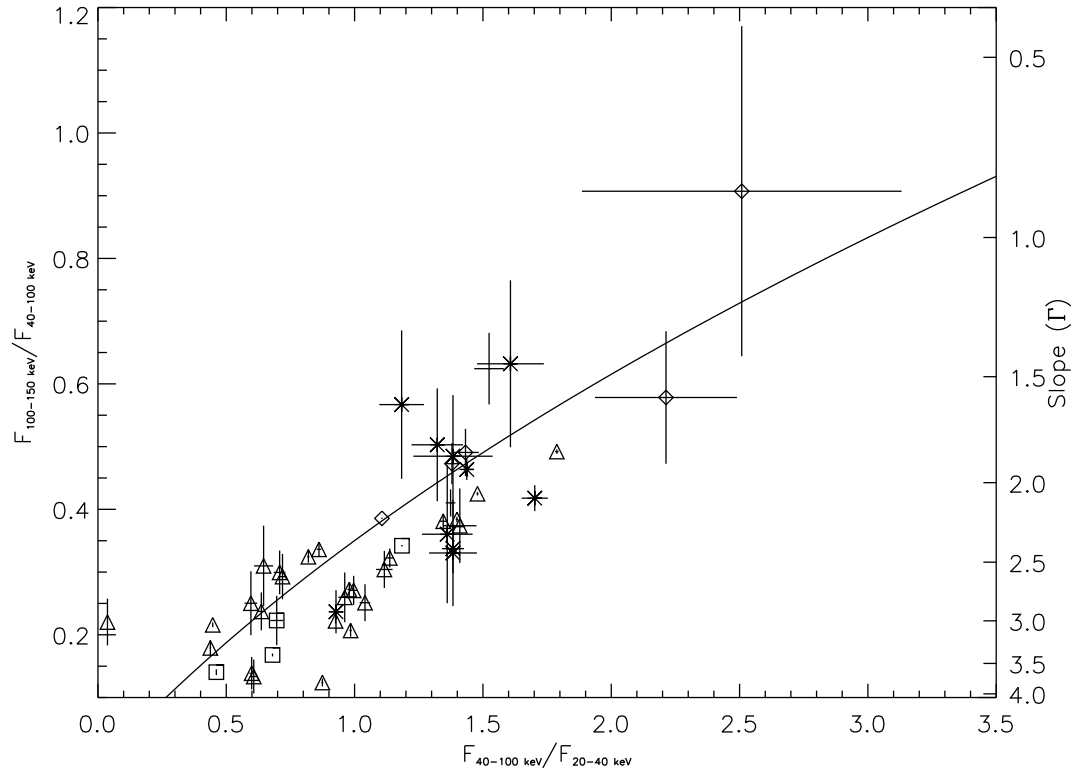


Fig. 1. | The High energy hardness ratio (100-150 keV / 40-100 keV) as a function of the low energy hardness ratio (40-100 keV / 20-40 keV). The stars are AGN, diamonds are PSR, triangles and squares are LMXB and HMXB and no symbol are unidentified. The curve is the locus of ratios as a function of photon slope (left-hand axis)

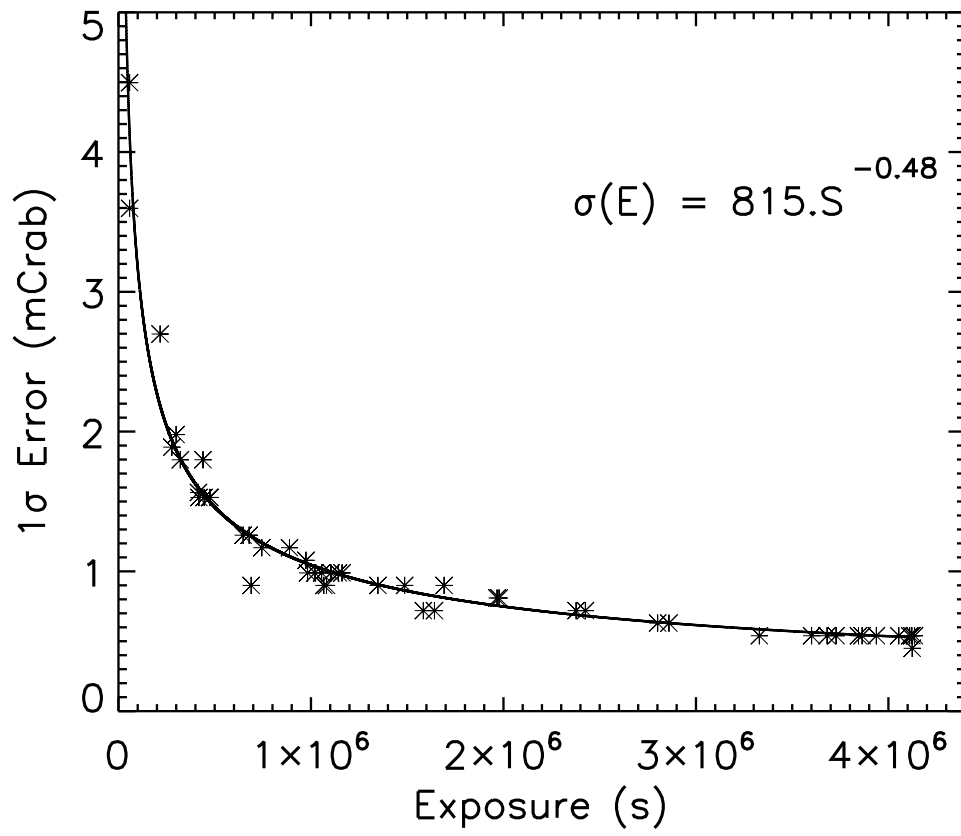


Fig. 2. | The error on the source fluxes as a function of source exposure. This relationship is used to compute the flux limit for the entire exposure map.

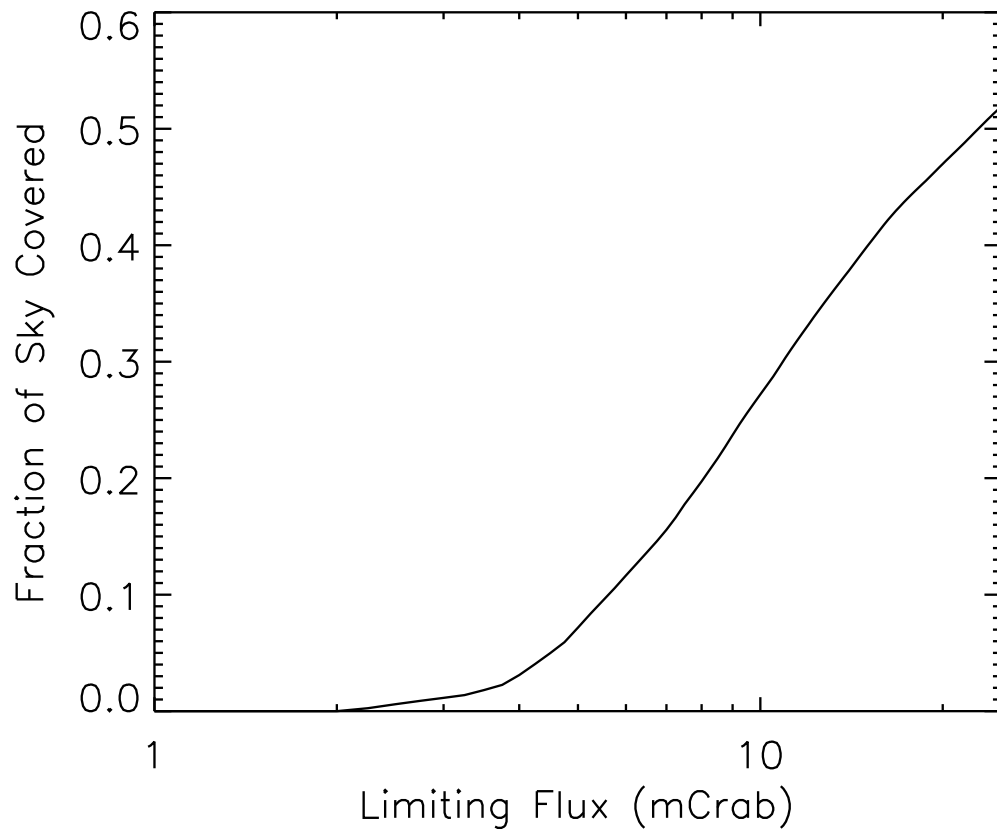


Fig. 3. | The all-sky fractional coverage as a function of (4) limiting flux.

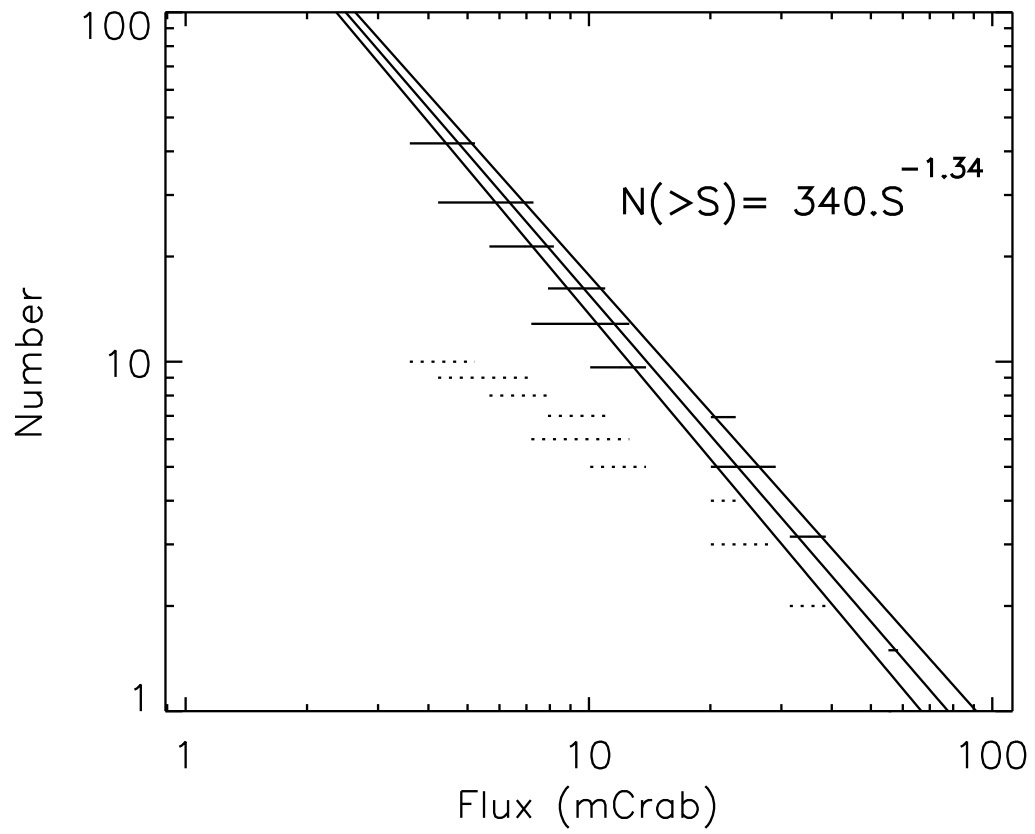


Fig. 4. | 100-150 keV full sky number-flux relationship for the 10 AGN in our sample. Data points for both before (lower, dotted) and after correction for exposure are shown as are the best-fit power law with 1 limits.

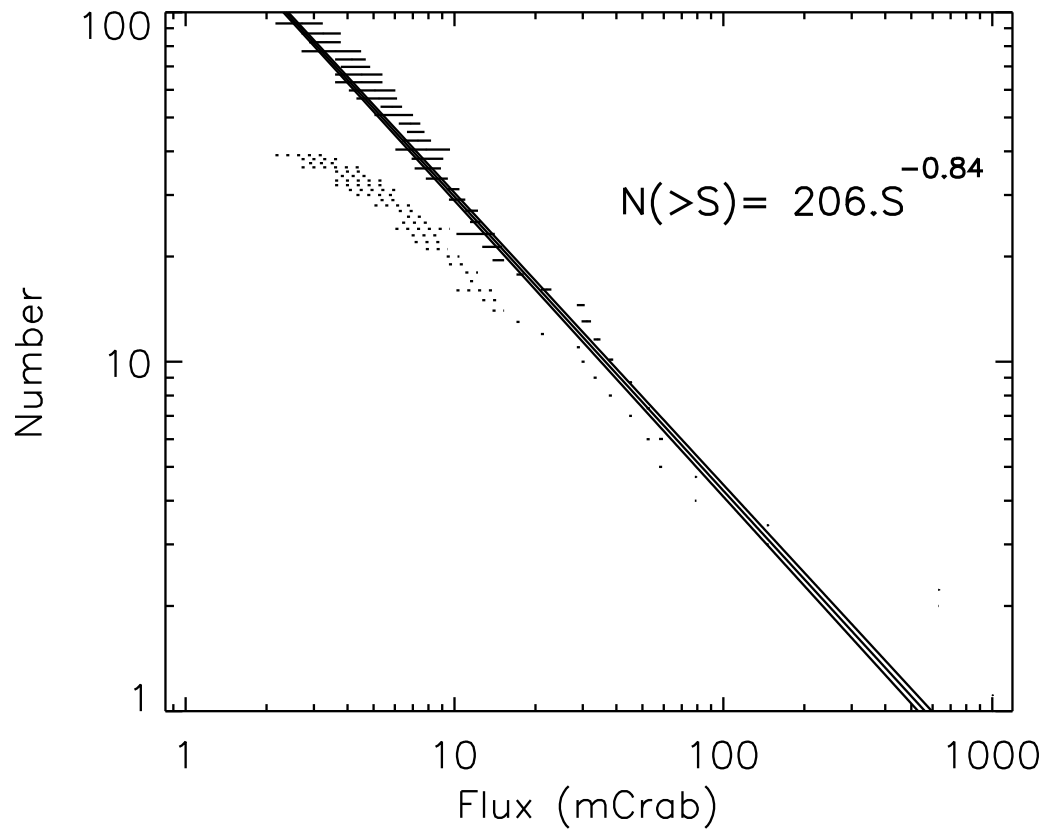


Fig. 5. | As Fig. 4, but for the 39 galactic sources in the sample.

TABLE 1
IBIS detections in (100–150)keV and (150–300)keV energy band

name	class	IBIS		IBIS		IBIS		IBIS		SA X		SA X		ref
		(20–40)		(40–100)		(100–150)		(150–300)		(100–150)		(150–200)		
		keV		keV		keV		keV		keV		keV		
m C rab		m C rab		m C rab		m C rab		m C rab		m C rab		m C rab		
4U 0142+ 61	AXP	1:5	0:3	3:4	0:5	8	2							(1)
Crab	PWN PSR	1000:0	0:4	1000:0	0:6	1000	2	1000	6	1000	3 ^(c)	1000	3	
MKN 3	AGN	4:2	0:2	6:1	0:4	10	2							
VelaPulsar	PWN PSR	6:74	0:09	8:4	0:1	10:3	0:7							
GS0836–429	LMXB TB	30:58	0:09	27:2	0:1	14:6	0:7							
NGC 4151	AGN Sey1.5	32:0	0:6	40	1	35	4			28:5 ^{+0:3} _{0:3} ^(b)		18:0 ^{+0:3} _{0:5}		(2)
NGC 4388	AGN Sy1	15:9	0:7	17	1	25	5							(3)
3C 273	AGN QSO	7:7	0:3	9:2	0:6	12	2			23:7	0:7 ^(a)	27	1	(4)
NGC 4507	AGN Sy1h	8:7	0:4	10:7	0:6	10	3							
NGC 4945	AGN Sey2	13:2	0:3	20:3	0:4	22	1			23:1 ^{+0:6} _{0:5} ^(b)				
CenA	AGN Sey2	36:5	0:2	47:4	0:4	57	2	65	6	49:5 ^{+0:3} _{0:3} ^(b)		52:0 ^{+0:5} _{1:0}		(5)
Cir galaxy	AGN Sy1h	13:6	0:2	11:4	0:3	7	1			3:4 ^{+1:1} _{0:5} ^(c)				
PSRB1509–58	PSR	8:5	0:2	11:0	0:3	14	1							(6)
XTE J1550–564	LMXB TB BH	70:8	0:2	114:4	0:3	146	1	155	4	115 ⁺¹ ₁ ^(a)		114:2 ^{+0:5} _{1:5}		(7)
4U 1608–522	LMXB TBA	14:3	0:2	7:7	0:3	5	1							
ScoX–1	LMXB Z	629:0	0:4	21:0	0:6	12	2							
4U 1630–47	LMXB TBHC	44:2	0:2	34:4	0:3	30	1	30	4	48:5 ^{+0:3} _{0:3} ^(a)		43:0 ^{+0:5} _{0:5}		(8)
4U 1636–536	LMXB BA	22:6	0:2	13:0	0:3	8	1							
OA0 1657–415	HMXB XP	78:6	0:2	42:5	0:3	7:3	0:9							
GX 339–4	LMXB TB BH	28:3	0:2	34:4	0:3	34	1	31	4	43:4 ^{+0:3} _{0:3} ^(b)		28:8 ^{+0:5} _{0:5}		(9)
4U 1700–377	HMXB	196:21	0:09	120:6	0:1	52:5	0:7	23	3					(10)
4U 1702–429	LMXB BA	16:1	0:2	10:3	0:3	8:0	0:9			10:2 ^{+0:3} _{0:3} ^(b)				
4U 1705–440	LMXB BA	23:7	0:2	13:0	0:3	4:5	0:9			14:2 ^{+0:3} _{0:3} ^(b)				
IGRJ17091–3624	BHC?	8:78	0:09	10:9	0:1	11:6	0:6							(11)
XTE J1720–318	LMXB TBHC	2:59	0:09	3:3	0:1	3:2	0:5							(12)
GRS1724–30	LMXB B A G	19:21	0:09	17:0	0:1	12:0	0:5			26:1 ^{+0:6} _{0:6} ^(b)				
GX 354–0	LMXB BA	39:17	0:09	15:5	0:1	7:2	0:5							
GX 1+ 4	LMXB XP	38:98	0:09	30:8	0:1	9:9	0:5			10:5 ^{+0:3} _{0:3} ^(b)				
SLX 1735–269	LMXB B	9:33	0:09	8:4	0:1	5:9	0:5							
1E 1740.7–294	LMXB BHC	35:84	0:09	45:3	0:1	45:1	0:5	37	2					(13)
KS1741–291	LMXB TB	5:64	0:09	4:9	0:1	3:3	0:5							
A 1742–294	LMXB TB	13:86	0:09	7:5	0:1	2:7	0:5							
IGRJ17464–3213	LMXB BHC	28:08	0:09	20:8	0:1	17:5	0:5	20	2					(14)
SLX 1744–299	LMXB B	8:31	0:09	5:4	0:1	4:1	0:5							
IGRJ17597–2201	LMXB BD	7:02	0:09	6:6	0:1	4:3	0:5							
GRS1758–258	LMXB BHC	53:58	0:09	71:6	0:1	78:9	0:5	70	2					(15)
SGR J1806–20	SGR	3:05	0:09	4:2	0:1	6:8	0:6			2:4	0:3 ^(a)	2:2	0:5	(16)
4U 1812–12	LMXB BA	25:6	0:2	26:3	0:3	22	1	18	4					(17)
GS1826–24	LMXB B	79:26	0:09	66:3	0:1	38:2	0:7	12	3	32:2 ^{+0:3} _{0:3} ^(b)				
PKS1830–211	AGN QSO	2:8	0:2	3:5	0:3	4:4	0:8							(18)
1RX 1832–33	LMXB BTG	10:81	0:09	10:9	0:3	8:6	0:8							
KES 73	SNR AXP	2:0	0:2	4:0	0:3	6	1			21	2 ^(a)	31	3	
4U 1909+ 07	HMXB T XP	14:3	0:2	9:0	0:3	5:2	0:9							
Aql X 1	LMXB B A T	9:6	0:2	5:6	0:3	4:5	0:9			3:6 ^{+1:1} _{0:8} ^(a)		3:3 ^{+1:0} _{0:6}		(19)
GRS1915+ 105	LMXB BH	260:8	0:2	105:4	0:3	59	1	47	4	82:6 ^{+0:2} _{0:2} ^(b)		55:5 ^{+0:2} _{0:1}		(20)
Cyg X–1	HMXB BH	665:7	0:3	712:5	0:4	632	2	522	6	950 ⁺³ ₃ ^(b)		870 ⁺⁵ ₅		(21)
EXO 2030+ 375	HMXB XPBeT	38:8	0:2	20:4	0:4	3:6	0:9							(22)
Cyg X–3	HMXB	204:1	0:2	85:1	0:3	31	1	20	5	18:0 ^{+0:3} _{0:3} ^(b)		12:1 ^{+0:5} _{0:5}		(23)
IGRJ21247+ 5058	AGN Sy 1?	5:6	0:2	7:0	0:4	6:0	1:5							

Note. | Class are according with Bird et al. 2006. Beppo-Sax fluxes in mCrab measured by PDS in the band 100–150 and 150–200 keV respectively. Only sources detected with signal to noise > 4 are reported. 1mCrab = $3.2 \cdot 10^{12} \text{ erg cm}^{-2} \text{ s}^{-1}$ in the 100–150 keV range. 1mCrab = $4.8 \cdot 10^{12} \text{ erg cm}^{-2} \text{ s}^{-1}$ in the 150–300 keV range.

The notes indicate the model used to fit Beppo-Sax data: (a) simple power law, (b) cut-off power law and (c) broken power law.

References. | (1) Kuiper et al. 2006; (2) Beckmann et al. 2005; (3) Beckmann et al. 2004; (4) Courvoisier et al. 2003; (5) Rotschild et al. 2005; (6) Shaw et al. (7) Stumer et al. 2005; (8) Tomasz et al., 2005 (9) Belloni et al. 2006; (10) Orr et al. 2004; (11) Capitanio et al. 2005; (12) Cadolle-Belet et al. 2004; (13) DelSanto et al. 2005; (14) Capitanio et al. 2004; (15) Pottschmidt et al. 2006; (16) Mereghetti et al. 2005; (17) Tarana et al. 2006; (18) De Rosa et al., 2005; (19) Molokov et al. 2004; (20) Hannikainen et al. 2005; (21) Cadolle-Belet et al. 2006; (22) Camerota et al., 2005 (23) Vilhu et al. 2003